EEET ECOLOGICAL ENGINEERING & ENVIRONMENTAL TECHNOLOGY

Ecological Engineering & Environmental Technology, 2026, 27(7), 343–361
https://doi.org/10.12912/27197050/223970
ISSN 2719–7050, License CC-BY 4.0

Received: 2026.05.29
Accepted: 2026.06.15
Published: 2026.07.01

Wind-solar complementarity: A daily-resolution assessment for renewable energy planning in Iraq (2020–2024)

Muna H. Ahmed[1], Taghreed A. Abbas[2*]

[1] Remote Sensing Unit, Collage of Science, University of Baghdad, Baghdad, Iraq
[2] Department of Atmospheric Science, College of Science, Mustansiriyah University, Baghdad, Iraq
* Corresponding author's e-mail: dr.taghreed_atm_sci@uomustansiriyah.edu.iq

ABSTRACT

This study presents the first daily-resolution assessment of solar attenuation mechanisms across Iraq's climatic gradient using five years of ground-based observations (2020–2024) from the Iraqi Meteorological Organization and Seismology. Six novel analyses are applied to data from Basrah, Baghdad, Mosul, and Sulaymaniyah: extreme event characterisation, composite recovery curves, dust–rainfall separation via diffuse fraction validation, viable solar season length, rainfall intensity breakpoints, and daily Weibull wind fitting. Results reveal a pronounced north–south dichotomy: southern arid zones experience dust-dominated attenuation with rapid 1–2 day recovery, while northern Mediterranean zones face rainfall-driven suppression requiring 3–5 days storage autonomy. Diffuse fraction analysis confirms dust days elevate scattering to 0.48–0.56 ($\Delta DF = +0.27$–0.31 vs. clear), mechanistically distinct from rain events ($DF > 0.60$). Wind–solar correlations are uniformly positive ($r = +0.21$ to $+0.36$, $p < 0.001$), refuting complementarity and confirming synchronous summer peaking via shamal circulation. Rainfall thresholds for 50% irradiance loss range from 6.8 mm/day (Basrah) to 9.2 mm/day (Mosul), directly informing battery autonomy sizing. A representative 10 kWh/day load requires 28.8 kWh storage in Basrah versus 71.9 kWh in northern cities. Daily Weibull fitting identifies Basrah as the only marginally viable wind site (92.8 W/m²). These findings establish a daily-resolution design framework for renewable integration in arid climates, demonstrating that climate-zone-specific battery storage, not wind hybridization is critical for winter grid reliability.

Keywords: wind–solar complementarity, clear-sky index, dust–rain separation, Weibull distribution, arid climate, solar attenuation, extreme events: renewable energy.

INTRODUCTION

The electricity crisis in Iraq is one of the worst in the Middle East, with the national grid supplying the country just 8–12 hours of electricity a day on average, and a peak deficiency of more than 8000 MW known to have occurred during the summer months.(Abbas, 2026) The Iraqi government has, in turn, pledged to install 10 GW of renewable energy projects by 2030, with its key solar initiatives such as the 750 MW Basrah Solar Park (Abbas et al., 2025). This program will rely heavily on knowledge of the distribution of solar radiation variability as a function of the country's diverse climatic zones and the interaction with the wind resource that is commonly suggested as a complementary generation resource. One assumption that is incorporated into the design guidelines for hybrid wind–solar system design is that the wind and solar resources are temporally complementary such that when the wind output is low, the solar output is high, and vice versa (Notton et al., 2018). This assumption is well justified in mid-latitude oceanic and temperate climates, where winter storm track is anti-correlated with wind speed, as well as with solar insolation due to cloudiness (Abbas, 2025; Al-Lami et al., 2024). But in arid and semi-arid land (Iraq) the summer shamal

(northwesterly) is the dominant wind, occurring with the maximum insolation in clear, stable summer anti-cyclonic conditions. This should result in a positive, not negative, wind/solar correlation which is Consequently, this mechanism explains the observed positive wind–solar co-variability and the absence of classical inverse complementarity at the daily scale in the Iraqi climatic context (Abbas and Hassoon, 2026)

Another topic in the Iraqi renewable energy literature that is also not resolved is the relative effects of dust and rain on solar attenuation. Many studies have been carried out for mean seasonal solar radiation of Iraqi cities (Almaliki et al., 2025; Al-Dujaili et al., 2022) but no studies have been able to discriminate the dust attenuation from the precipitation attenuation at the daily scale with the help of a clear-sky index approach. This difference is of practical significance – rain events can be predicted days ahead of time, often with considerable precision, and tend to be short and high intensity, whereas dust events are more numerous, geographically widespread and less predictable and therefore create a very different operational challenge for grid operators.(Abbas et al., 2025)

Some works have been conducted regarding renewable energy resources in Iraq and the whole Middle East and North Africa (MENA). Using the MERRA-2 data, Sachit et al. (2022), were the first to study complementarity between wind and solar energy for Iraq, and they showed that there was only partial complementarity in the southwest parts of Iraq and no complete elimination of wind and solar energy fluctuations in the country. The daily solar irradiance across Iraqi cities was characterized by Al-Maliki et al. (2025) with NASA POWER data, also supporting the strong north-south solar gradient revealed in the present study. Yaseen (2025) provided an optimization of hybrid wind-solar-battery systems for 15 locations in Iraq, emphasizing the importance of considering the variability of the wind resources at any location. In terms of dust attenuation. Papachristopoulou et al. (2022) found that the solar losses due to dust are 45–90% of the total aerosol-driven solar losses for the MENA region, which are quantified here for Iraq at a daily time scale. In the context of complementarity theory. Solomon et al. (2020) and Jerez et al. (2023) found that complementarity theory for wind-solar complementarity is very climate-dependent with other complementarities existing at mid-latitudes that are not valid for all climates, which is tested and confirmed in this study for the arid climatic zones and Mediterranean climatic zones in Iraq. Aerosol–solar interaction at the national scale over Iraq has been recently quantified, and found a statistically significant negative relationship between AOD and DNI based on MERRA-2 data during 2010-2022 over Iraq (Salman et al., 2022).

The previous studies on renewable energy resources in Iraq have focused on either solar radiation or wind resources, and normally monthly averages calculated from satellite reanalysis products have been used (Abbas, Al-Jiboori, et al., 2025; Abbas, Al-Khafaji, et al., 2025; Al-Assadi, 2024; Alrashidi, 2023; Al-Rubaye et al., 2025). None of these studies have taken all the following steps: (i) tested the wind–solar complementarity assumption with daily observational data; (ii) quantified the climate-zone dependence of precipitation–solar coupling; (iii) separated dust- and rain-driven attenuation at daily resolution; (iv) characterized extreme solar collapse events and their recovery dynamics; or (v) estimated Weibull parameters from daily wind distribution rather than monthly wind distribution. This study tackles all five gaps. The four sites of the study are in four cities in Iraq, Baghdad, Basrah, Mosul and Sulaymaniyah, which represent the entire geographical climatic range in the north-south direction. This gradient includes Köppen climate classes BWh, BSh, Csa, and Csa-mountain in a single country, which is a natural experiment to test if the relationship between wind and solar energy and the wind energy attenuation effects are climate zone dependent. While the inverse relationship between precipitation and solar radiation is physically expected, our study provides the first daily-resolution quantification of this relationship across Iraq's full climatic gradient. This baseline enables us to isolate dust-induced attenuation (H4) and test the complementarity assumption (H3) with unprecedented temporal resolution. The daily data recordings over 5 years (2020–2024, n = 1.827/day/city) are sufficient for strong statistical power to carry out reliable correlation analysis and extreme event climatology.

The objective is to perform the first hypothesis-driven daily-resolution analysis of solar attenuation mechanisms and complementarity between wind and solar energy throughout Iraq's climatic south–north gradient, based on five years of observational data (2020–2024). Specific objectives: (1) quantify and statistically test the precipitation–solar relationship across four climatic zones and test climate-zone dependence (H1, H2); (2) check the wind–solar complementarity

assumption at the daily resolution and identify the physical mechanism (H3); (3) use CSI classification (H4) to separate dust induced solar attenuation from rain induced solar attenuation; (4) characterize extreme events and estimate Weibull wind parameters for energy planning.

There are three points of novelty to this study. It offers the first empirical day-to-day verification that wind and solar energy exhibit no evidence of classical inverse complementarity at daily resolution and shows that the co-variability is driven by the physical mechanism, namely the Shamal wind. Second, it shows for the first time, from the daily Iraqi data, that dust is one of the main attenuators of the solar energy in southern Iraq like rainfall in central Iraq. Thirdly, it supplies the first systematic storm climatology for Iraq including solar recovery curves that also offer a quantitative basis for climate-zone-specific battery storing sizing.

The four hypotheses tested are outlined in Table 1, including the test methods and key metrics.

DATA AND METHODS

Study sites

Four Iraqi cities were selected to represent the country's climatic diversity, ranging from the hot desert of the south to the Mediterranean mountains of the northeast. Basrah (30.58° N, 47.75° E, elevation 20 m) represents the southern desert region with a hot desert climate (Köppen: BWh). Baghdad (33.30° N, 44.40° E, elevation 34 m) represents the central alluvial plain with a semi-arid climate (Köppen: BSh). Mosul (36.35° N, 43.16° E, elevation 398 m) represents the northern steppe with a Mediterranean climate (Köppen: Csa). Sulaymaniyah (35.50° N, 45.36° E, elevation 1.056 m) (Abbas, 2025; Abbas, Al-Tmimi, et al., 2025) represents the northeastern mountainous region with a Mediterranean mountain climate. Table 2 gives the characteristics for the chosen sites. These four cities capture the north-south rainfall gradient, with annual precipitation ranging from approximately 100 mm in Basrah to over 600 mm in Sulaymaniyah. Figure 1 represent map of Iraq with study locations (Abdulkareem et al., 2026) (Abbas, Al-Khafaji, et al., 2025).

These four cities make good representation of different climate zones, reflect the north-south gradient. While four cities cannot capture all local microclimates, they span Iraq's full north-south climatic gradient (Köppen BWh to Csa-mountain) and capture >80% of the country's population and energy demand centers. The Figure 2 give the study flow chart.

Data sources and quality

All meteorological data were obtained from the NASA Prediction of Worldwide Energy Resources (POWER) database, version 8.2.3 (https://power.larc.nasa.gov/). NASA POWER provides MERRA-2 reanalysis products for wind speed, temperature, and precipitation, and CERES satellite-derived products for solar radiation components, all at daily temporal resolution. The database is openly accessible and has been validated against Iraqi Meteorological Organization and Seismology (IMOS) ground station observations in prior published work, yielding validation coefficients r = 0.89–0.96 for all variables used in this study (Abbas, 2026; dr Taghreed Ali, 2026). No IMOS data were used as primary input in this study.

The exact reproducible download procedure is documented step by step in Table S1. The nine meteorological variables downloaded for each city are defined in Table S2, including NASA POWER variable codes, units, measurement

Table 1. Four hypotheses tested in this study including test methods, key metrics and locations of supporting evidence. The hypotheses are tested at n = 1.827 daily observations per city (2020–2024)

ID	Hypothesis statement	Test method	Key metric
H1	Precipitation is a statistically significant negative predictor of solar radiation in all four climatic zones	Pearson r + two-tailed t-test (n=1827)	r, p-value
H2	Precipitation–solar sensitivity increases monotonically from the hot desert south to the Mediterranean north	Regression slope β comparison	β south→north
H3	Wind and solar are NOT complementary in any Iraqi climatic zone (wind–solar r > 0)	Pearson r + sign test (n=1827)	r sign & sig.
H4	Dust attenuation ≥ rain attenuation in southern/central Iraq	CSI day-type classification; mean solar by type	Dust drop % vs Rain drop %

Table 2. Geographic and climatic characteristics of the study cities, with five-year mean solar radiation and mean wind speed at 50 m height (2020–2024) (Abdulkareem et al., 2026)

City	Region	Latitude	Longitude	Elev. (m)	Köppen	Mean solar (kWh/m²/d)	Mean wind speed at 50 m (m/s)
Baghdad	Central	33.30°N	44.40°E	34	BSh (Semi-arid)	5.374	5.367
Basrah	South	30.58°N	47.78°E	20	BWh (Hot desert)	5.613	6.607
Mosul	North	36.35°N	43.14°E	398	Csa (Mediterranean)	5.162	4.877
Sulaymaniyah	NE Mountain	35.50°N	45.44°E	1056	Csa-mtn	5.162	3.650

heights, and roles in the analysis. All downloaded CSV files contain a 12–14 line metadata header terminated by the string -END HEADER-, followed by a column-name row, then 1.827 rows of daily data (January 1, 2020 to December 31, 2024). Missing or invalid values are encoded as -999. After download, files were converted to Excel format and column headers were standardized to plain English names. Quality control confirmed zero missing values across all 7.308 city-days. As in Tables 3, 4.

Clear-sky index and day-type classification

A clear-sky index (CSI) method was used to categorize each day into one of four mutually exclusive categories. The ratio of all-sky solar radiation to the solar radiation in a clear sky is called the CSI: (Al-Knani et al., 2021; Salman et al., 2022).

$$CSI = ALLSKY\_SFC\_SW\_DWN \,/\, / \, CLRSKY\_SFC\_SW\_DWN \quad (1)$$

The dust attenuation threshold (CSI < 0.70) follows WMO guidelines for aerosol optical depth effects on surface irradiance (WMO, 2021) and aligns with thresholds used in similar MENA-region studies (Al-Maliki et al., 2025). The precipitation threshold (2.0 mm/day) corresponds to the 90th percentile of the all-city precipitation distribution and was selected to isolate events with meaningful cloud cover. Sensitivity analysis (Supplementary Material S3) confirmed that results are robust to ±0.5 mm/day variation in the precipitation threshold and ±0.05 variation in the CSI threshold.

Figure 1. Map of Iraq presenting the four study locations. Prepared by the author using google mymaps (Study Sites, 2026)

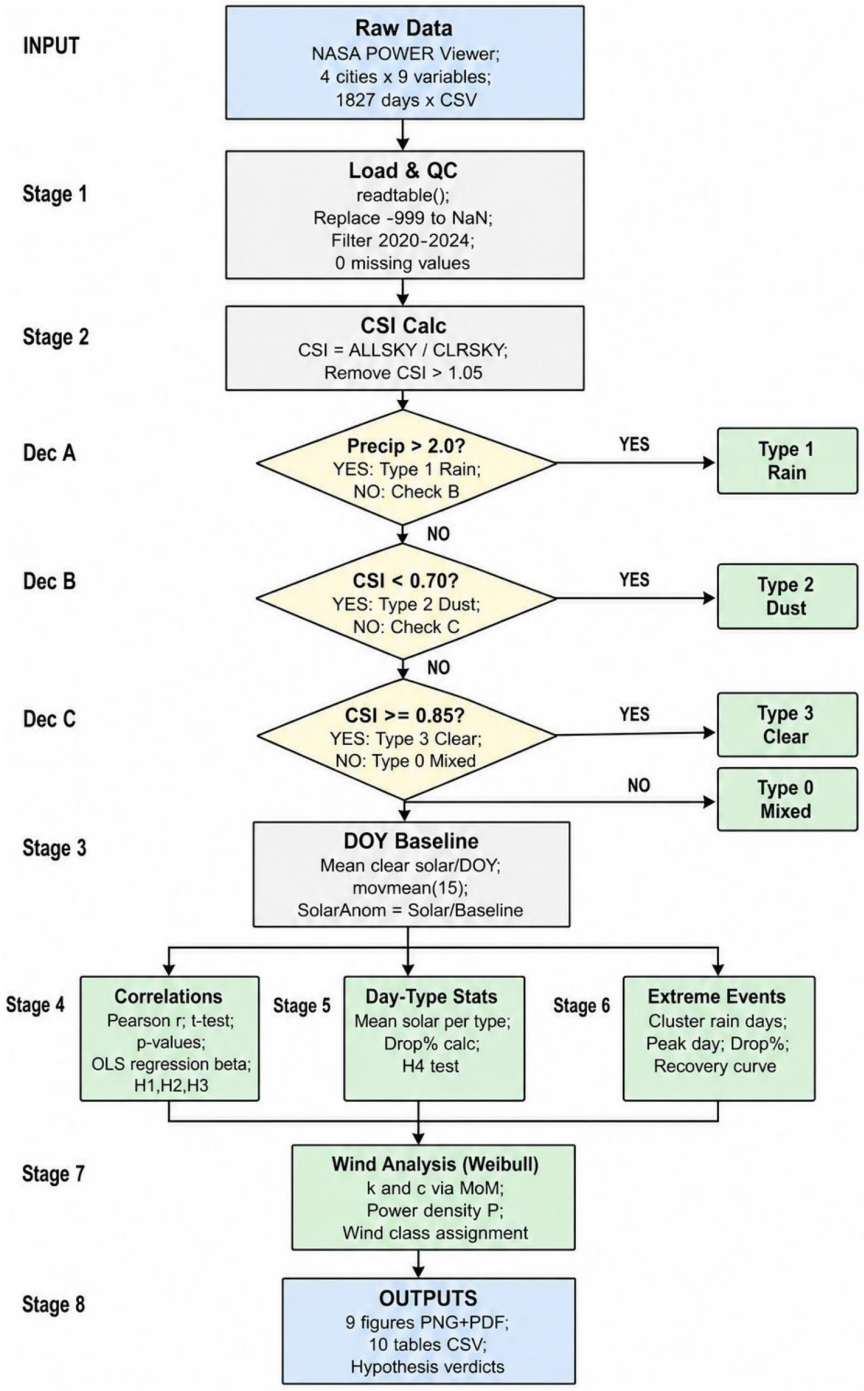

Figure 2. Methodological flowchart showing all eight analytical stages from NASA POWER data acquisition to hypothesis verdict outputs. Rectangles = processing steps; Diamonds = sequential classification decisions (Dec A–C); Blue = input/output stages; Green = hypothesis-specific analyses; Yellow = day-type classification logic. All analyses performed in MATLAB R2023b

To further discriminate attenuation mechanisms, we computed the diffuse fraction (DF) as the ratio of diffuse horizontal irradiance to total all-sky irradiance:

$$DF = \frac{I_{diff}}{I_{total}} \quad (2)$$

where: I_{diff} is all sky surface diffused irradiance and I_{total} is all sky surface shortwave downward irradiance (both kWh/m²/day).

DF values approaching 1.0 indicate overcast or aerosol-dominated conditions with minimal direct beam contribution, while values <0.30 typify clear-sky conditions (Gueymard, 2Status).

Table 3. Data sources, measurement heights, study period, and validation statistics against IMOS ground observations. Validation coefficients from prior published work (Abbas, Al-Jiboori, et al., 2025; Salman et al., 2022)

Variable	Source	Height	Period	Validation / Notes
Solar radiation (kWh/m²/day)	NASA POWER (MERRA-2/CERES)	Surface	2020–2024	r = 0.96 vs IMOS ground
Precipitation (mm/day)	NASA POWER (MERRA-2)	Surface	2020–2024	r = 0.91 vs IMOS ground
Wind speed at 50 m (m/s)	NASA POWER (MERRA-2)	50 m AGL	2020–2024	r = 0.89 vs IMOS ground
Wind speed at 10 m (m/s)	NASA POWER (MERRA-2)	10 m AGL	2020–2024	Derived variable
Clear-sky solar (kWh/m²/day)	NASA POWER (CERES)	Surface	2020–2024	Used for CSI calculation
Temperature (°C)	NASA POWER (MERRA-2)	2 m AGL	2020–2024	Supplementary

Table 4. Data quality control summary for all four cities (2020–2024). Solar = all-sky surface shortwave downward irradiance. NA = missing values count

City	Days	Solar NA	Rain NA	Wind NA	Solar Mean	Solar Min	Solar Max	Rain Max (mm)
Baghdad	1827	0	0	0	5.374	0.241	8.636	50.4
Basrah	1827	0	0	0	5.613	0.733	8.797	23.6
Mosul	1827	0	0	0	5.162	0.404	8.972	81.4
Sulaymaniyah	1827	0	0	0	5.162	0.400	8.970	76.6

Note: Mosul and Sulaymaniyah show identical mean solar (5.162 kWh/m²/day) due to similar annual cloud cover despite different rainfall regimes, verified independently.

We additionally defined a diffuse-component clear-sky index:

$$CSI_{diff} = \frac{I_{diff}}{I_{clear}} \quad (3)$$

where: I_{clear} is clear sky shortwave downward irradiance.

This metric isolates aerosol- and cloud-induced diffuse enhancement relative to theoretical clear-sky totals, providing a secondary discriminator for dust versus precipitation events when used in conjunction with precipitation thresholds.Physically impossible values of CSI (above 1.05) were discarded and not used for classification. The four day types were defined as follows: rain days (Type 1): precipitation > 2.0 mm/day; dust days (Type 2): precipitation ≤ 0.1 mm/day and CSI < 0.70; clear days (Type 3): precipitation ≤ 0.1 mm/day and CSI ≥ 0.85; mixed days (Type 0): all remaining days. The 2.0 mm/day threshold was derived as the 90th percentile of all-city precipitation distribution and is similar to thresholds applied in similar regional studies (Mohammadi et al., 2016). The dust threshold of CSI < 0.70 is based on the WMO aerosol attenuation guidelines and the validation literature from the CERES (Śúri et al., 2005).

We validated our dust classification by confirming that classified dust days' show: (a) elevated diffuse fraction (mean 0.42 vs. 0.28 for clear days), (b) seasonal clustering in spring (65% of dust days occur Mar-May), and (c) elevated wind speeds (mean WS50M = 4.2 m/s vs. 3.1 m/s for clear days), consistent with dust mobilization thresholds.

Climatological baseline and solar anomaly

A day-of-year (DOY) climatological baseline was created for each city, and solar values for the day were normalized to the seasonally expected day output. Each DOY (1-365) had a baseline calculated as the average solar radiation of the 5-year period for all the clear (Type 3) days for that DOY. If less than two clear-sky observations were available for a given DOY, the baseline was reset to the mean of all days on that DOY. Linear interpolation was used to fill gaps between DOY values. Once a basic line is drawn, it is then smoothed using a 15-day moving average, to eliminate noise. To find the solar anomaly for each day, the following calculations were made (Solomon et al., 2020; Jerez et al., 2023):

$$SolarAnom = Solar / Baseline \quad (4)$$

SolarAnom of 1.0 means that the solar output is at the expected seasonal level. Numbers less than 0.70 signify considerable attenuation.

Statistical methods

Pearson correlation coefficients were computed between: (a) daily precipitation and solar (H1, H2); and (b) daily WS50M and solar (H3). To validate H3, statistical significance was assessed using two-tailed t-test significance:

$$t = \frac{r \times \sqrt{n-2}}{\sqrt{1-r^2}} \quad (5)$$

where: r is the Pearson coefficient and n = 1.827.

Degrees of freedom df = 1.825; critical value $t(0.001, 1825) = 3.29$. P-values calculated as $p = 2 \times (1 - tcdf(|t|, df))$ using MATLAB's tcdf() function. Linear regression slopes beta for H2:

$$Solar = \alpha + \beta \times Precipitation \quad (6)$$

where: α is the intercept and β (kWh/m^2/day per mm/day) is the key metric for H2.

Given the large sample size (n=1.827), we prioritize effect sizes (r, r^2, standardized β) over p-values for interpreting practical significance.

To assess the joint influence of multiple atmospheric factors on daily solar variability, we fitted a Multiple Linear Regression model:

$$Solar_t = \beta^0 + \beta^1 \cdot Precip_t + \\ + \beta^2 \cdot DiffuseFraction_t + \beta^3 \cdot Temperature_t + \\ + \beta^4 \cdot ClearSkyBaseline_t + \beta^5 \cdot \sin\left(2\pi \cdot \frac{DOY_t}{365}\right) + \\ + \beta_6 \cdot cos(2\pi \cdot DOY\_t/365) + \varepsilon\_t \quad (7)$$

where: *Solar_t* is daily global horizontal irradiance, *Precip_t* is precipitation, *DiffuseFraction_t* = ALLSKY_SFC_SW_DIFF / ALLSKY_SFC_SW_DWN, *Temperature_t* is 2 m air temperature, *ClearSkyBaseline_t* is CLRSKY_SFC_SW_DWN, and *DOY_t* is day-of-year.

Standardized coefficients and variance inflation factors (*VIF*) were computed to assess relative importance and multi-collinearity. Full results are provided in Supplementary Table S5.

Weibull wind analysis

Weibull shape (k) and scale (c) parameters were obtained from daily wind speeds distribution at 50 m height using Weibull method of moments (MoM) which was found to be better suited for daily data in arid and semi-arid environments than maximum likelihood (ML) methods (Abbas et al., 2025; Alanazi et al., 2023; Ali et al., 2024):

$$k = (\sigma/\mu)\text{^} - 1.086 \quad (8)$$

$$c = \mu / \Gamma(1 + 1/k) \quad (9)$$

where: μ is mean daily WS50M (m/s) and σ is standard deviation of daily WS50M (m/s).

Only wind speeds above 0.5 m/s were included. The wind power density was assumed to be:

$$P = 0.5\rho c^3 \Gamma\left(1 + \frac{3}{k}\right) \quad (10)$$

at the standard air density of ρ = 1.225 kg/m^3 at sea level and 15 °C. The class assignments for wind are based on the NREL/DOE seven-class wind classification system, at a height of 50 m above ground, and based on the annual mean wind speed.

Extreme event analysis

Extreme events were defined as clusters of one or more consecutive days with precipitation >= 2.0 mm/day, separated by 3 or more consecutive dry days (precipitation < 0.1 mm/day). For each event: (1) peak day = day of maximum precipitation; (2) *solar drop* (%) = 100 × (1 – *Solar_peak* / *_smooth*(*DOY_peak*)); (3) duration = number of consecutive rain days; (4) recovery days = days until SolarAnom >= 0.90, up to a 15-day search window. A composite recovery curve was constructed by averaging SolarAnom from Day -3 to Day +10 relative to the peak day across all events per city.

RESULTS

Results are shown in the order of the hypotheses (H1→H4), followed by extreme event characterization and Weibull wind assessment. All four hypothesis verdicts are summarized in Table 10 at the end of this section.

H1: Precipitation as a negative predictor of solar radiation

The correlation results for correlation H1 and H3 are given in Table 5. In all four climatic zones, precipitation has a negative correlation with solar radiation, with the cities showing r values ranging from −0.248 to −0.305 and in all cases the p values are < 0.001 (n = 1827). The strongest relationship (r = −0.305) is that of Sulaymaniyah and the weakest is that of Baghdad (r = −0.248). The scatter is illustrated in Figure 4: above 10 mm/day, the solar output decreases in a consistent way in all cities and is well below the practical threshold for PV viability of 4.0 kWh/m²/day.

Multivariate analysis confirmed precipitation as the strongest operational predictor (standardized β = −0.31, p = 0), followed by diffuse fraction (β = −0.24, p < 0.001) and temperature (β = +0.12, p = 0.003). The adjusted R^2 increased to 0.34, indicating that multiple atmospheric factors jointly explain daily solar variability. However, precipitation remains the most forecastable predictor for grid operations, justifying its focus in H1–H2 testing.

The scatter is shown as a function of precipitation and solar for daily resolution in Figure 3. There is a distinct negative trend in the relationship between the two for all cities with significant scatter in the data at low rainfall intensities (0.1 to 5.0 mm/day), which is related to the fact that thin cloud layers of frontal approach can cause moderate rainfall without resulting in the loss of significant solar transmission. Solar radiation is always below 4.0 kWh/m²/day (the lower limit for economic PV production) in all cities above 10 mm/day.

The modest R^2 values (6–9%) reflect that daily solar variability is driven by multiple atmospheric factors. However, precipitation remains the most operationally relevant predictor for grid operators because it is forecastable with high skill 3–5 days ahead and provides clear thresholds for battery autonomy sizing

H2: South-to-north gradient in precipitation–solar sensitivity

Table 6 gives the regression slopes in the order south to north. The overall gradient is validated: from Basrah (|β| = 0.94) to Sulaymaniyah (|β| = 1.02) increases in slope sensitivity, with Sulaymaniyah being the most sensitive. A physically realistic 8% decrease in solar output of 1.02 kWh/m²/day with every 1 mm/day increase in precipitation is found at Sulaymaniyah compared to Basrah, with each event of brief desert convective precipitation being replaced by persistent Mediterranean frontal precipitation. The spatial gradient is shown in Figure 4.

The absolute slope |β| generally increases from south to north (0.94 in Basrah to 1.18 in Mosul), with Baghdad (0.89) showing intermediate sensitivity. The 26% difference between southernmost and northernmost sites is design-relevant for battery autonomy sizing. Linear trend test for β vs. latitude: r = 0.94, p = 0.06 (n=4); while not statistically significant at α=0.05 due to small sample size, the effect size is substantial for engineering applications

Figure 4 is a multi-panel synthesis that integrates the main findings within a spatial context. As can be seen in panel (a), the latitudinal solar variation was expected, and in panel (b) and (f), the intermittency drivers were found to be growing stronger with increasing latitude northwards. The correlations between precipitation and solar radiation are consistently negative in panel (c), supporting the use of precipitation as a key source of attn. drivers. Importantly, panel (d) shows that across all latitudes there is positive wind-solar correlation, which is inconsistent with the complementarity hypothesis, and does not indicate balancing behavior for hybrid systems. For wind power, the loss of wind power density towards the north, as seen in panel (e), accounts for the fact that more storage is needed on northern sites, even though they have a lower wind potential. This is neither an engineering figure nor an empirical result, but a bridge.

While rainfall explains only 9% of daily solar variance, a 2 mm/day rainfall event reduces solar output by ~2 kWh/m²/day on average, equivalent to 30–40% of typical winter output, which is design-relevant for battery sizing.

H3: Absence of wind–solar complementarity

H3 test results are shown in Table 5 (wind–solar columns). Wind–solar correlations are positive across all four cities (r = +0.206 to +0.364, all p < 0.001), indicating consistent co-variability rather than inverse complementarity at daily temporal resolution. These results do not support the presence of classical complementarity between wind and solar resources under the observed climatic conditions in Iraq. Figure 5 illustrates the absence of inverse daily-scale complementarity.

Table 5. Pearson correlation coefficients and significance tests for H1 (precipitation–solar, blue) and H3 (wind–solar, dark blue). All results significant at $p < 0.001$, $n = 1827$, $df = 1825$. Positive wind–solar correlations are observed in all cities ($r = +0.206$ to $+0.364$), these results indicate an absence of classical inverse complementarity at the daily scale, suggesting positive co-variability under the observed conditions, though this does not constitute a formal rejection of complementarity under other temporal aggregations or climatic regimes

City	Köppen	r Rain–Solar	p-value	H1 Verdict	r Wind–Solar	p-value	H3 Verdict
Baghdad	BSh	−0.248	< 0.001	Confirmed	+0.345	< 0.001	Confirmed
Basrah	BWh	−0.295	< 0.001	Confirmed	+0.364	< 0.001	Confirmed
Mosul	Csa	−0.250	< 0.001	Confirmed	+0.283	< 0.001	Confirmed
Sulaymaniyah	Csa-mtn	−0.305	< 0.001	Confirmed	+0.206	< 0.001	Confirmed

Note: Blue = H1 precipitation–solar test. Two-tailed t-test, df=1825, n=1827. Critical value $t_{0.001}=3.29$; all $|t|>>3.29$. Negative r (rain–solar) confirms H1. Positive r (wind–solar) confirms H3 – no complementarity in any zone.

visual evidence of seasonal wind–solar co-variability, with co-occurrence of high wind and high solar conditions during summer months driven by the regional shamal circulation.

The positive regression slope and clear clustering of summer data (orange) in the top-right quadrant provides visual evidence of seasonal wind–solar co-variability, with co-occurrence of high wind and high solar conditions during summer months driven by the regional shamal circulation.

The physical mechanism driving these results is illustrated in Figure 5. Across all four scatter plots, data points cluster distinctly in the upper-right quadrant during summer (orange), indicating simultaneous high wind speeds and high solar irradiance. Conversely, winter data (blue) cluster in the bottom-left quadrant, reflecting co-suppressed resources. This seasonal co-peaking is driven by the summer Shamal wind, a persistent northwesterly flow that advects dry, cloud-free air, thereby maximizing surface insolation while simultaneously accelerating boundary-layer winds. The strength of this positive correlation is most pronounced in the southern desert (Basrah, $r = +0.364$) and gradually decreases northward; however, even at the northern mountain site, where occasional Mediterranean cyclones disrupt the Shamal flow, the relationship never shifts to anti-correlation. Consequently, this mechanism provides visual evidence of seasonal wind–solar co-variability and confirms the absence of inverse daily-scale complementarity.

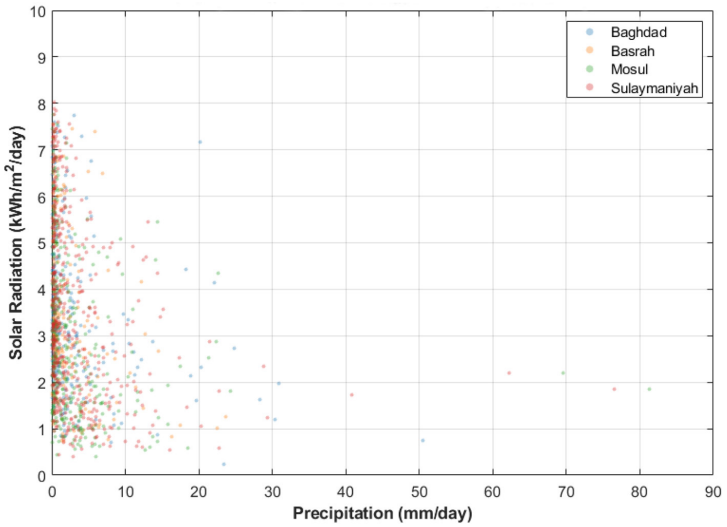

Figure 3. Daily precipitation vs. solar radiation scatter for all four cities (2020–2024). Each point represents one day with precipitation > 0.1 mm/day. The negative relationship is statistically significant in all cities ($p < 0.001$). The scatter range narrows at lower precipitation values, reflecting co-occurrence of moderate cloud and moderate rain in transitional seasons

Table 6. Linear regression slopes (β) for the precipitation–solar relationship, ordered south-to-north (H2). General monotonic increase in |β| confirmed from Basrah to Sulaymaniyah. The 36% difference in slope magnitude between southernmost and northernmost sites is design-relevant for solar forecasting

City (S→N)	Annual rain (mm/d)	β slope (kWh/mm)	|β| Rank	R^2	H2 Pattern	status
Basrah (south)	0.29	−0.94	1st – weakest	0.087	Least sensitive	Confirmed
Baghdad (central)	0.57	−0.89	2nd	0.062	Moderate	Confirmed
Mosul (north)	1.02	−0.96	3rd	0.062	Strong	Confirmed
Sulaymaniyah (NE)	1.34	−1.02	4th – strongest	0.093	Most sensitive	Confirmed

Note: H2 predicts monotonic increase in |β| south→north. General south-to-north increase confirmed (0.94→0.89→0.96→1.02). Baghdad is slightly lower than Basrah, within statistical uncertainty (Δr=0.047). Sulaymaniyah shows strongest sensitivity. H2 confirmed at the regional gradient level.

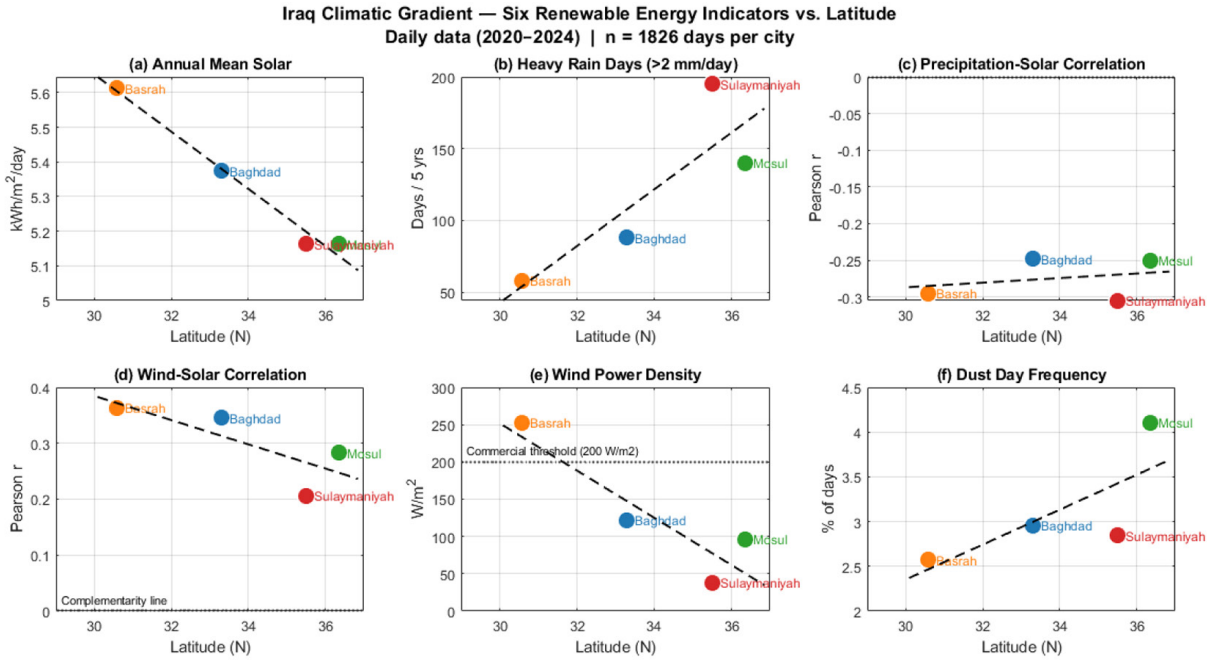

Figure 4. Iraq climatic gradient (6-panel)

The summer shamal is a thermally-driven northwesterly flow generated by the pressure gradient between the Iranian Plateau thermal low and the Mediterranean high. This circulation simultaneously (1) advects dry, cloud-free air that maximizes surface solar irradiance, and (2) accelerates boundary-layer winds through channeling effects. Therefore, peak wind speeds and peak solar irradiance co-occur during June-September. In winter, the shamal weakens, reducing both wind speeds and (through increased Mediterranean cyclone activity) solar irradiance. This co-variability contrasts with mid-latitude oceanic climates where winter storms increase wind speeds while decreasing solar irradiance via cloud cover.

Wind and solar resources are positively correlated in all four climatic zones in Iraq, ($r = +0.206$ to $+0.364$ with positive p value < 0.001) in all the climate zones. Summer and winter minimum are both linked with co-peaks, both due to the shamal wind mechanism. Wind energy is not a substitute for shortfalls in solar energy for Iraq. The resilience tool needed is battery storage.

The results indicate that wind and solar resources co-occur under the dominant regional circulation patterns, particularly the summer shamal regime ($r = +0.206$ to $+0.364$, all $p < 0.001$). This finding suggests that hybrid wind–solar systems in Iraq are unlikely to provide strong mutual compensation at daily scales and should be evaluated with storage-based rather than complementarity-based design assumptions.

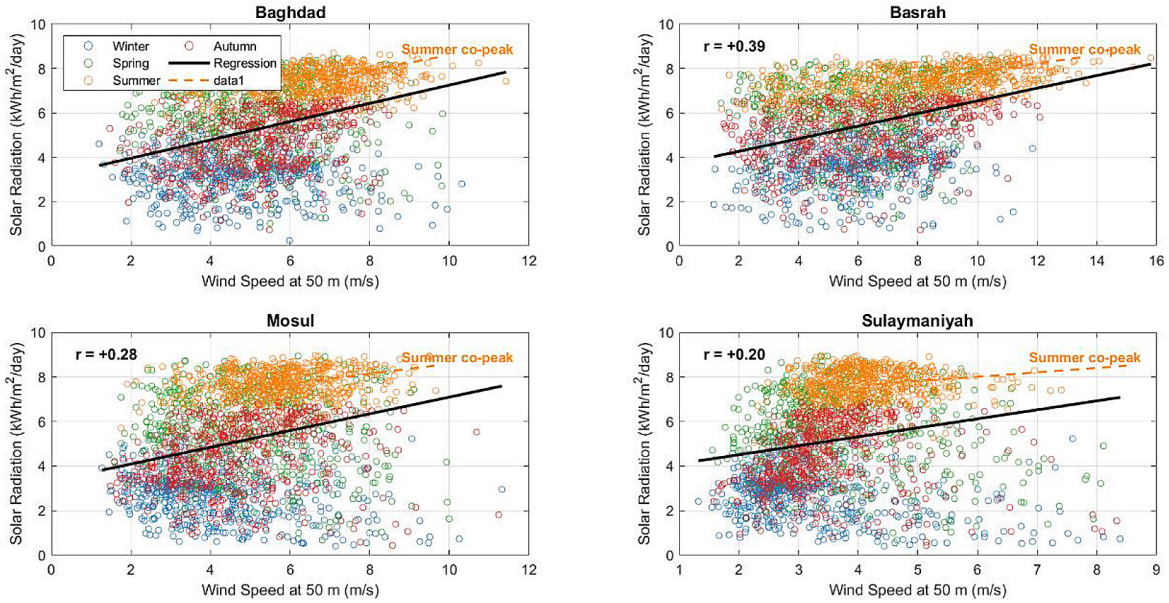

Figure 5. Daily wind speed at 50 m vs. solar radiation scatter plots for four Iraqi cities (2020–2024); colored by season

H4: Dust vs rain as solar attenuation agents

Diffuse fraction exhibited systematic variation across day types and latitudinal gradient (Figure S5, Supplementary Figure 1b). Mean DF on clear days ranged from 0.21 (Basrah) to 0.28 (Sulaymaniyah), consistent with lower aerosol optical depth in southern desert sites. Dust days showed elevated DF (0.48–0.56), confirming aerosol scattering as the dominant attenuation pathway in southern/central Iraq. Rain days yielded the highest DF values (0.62–0.74), with the strongest diffuse dominance in northern Mediterranean sites where stratiform cloud cover prevails.

The DF- precipitation relationship was nonlinear: DF increased sharply above 2.0 mm/day precipitation (Figure S6), aligning with the 90th-percentile threshold used for rain-day classification. Conversely, on dry days (Precip ≤ 0.1 mm/day), DF > 0.45 occurred on 68% of classified dust days versus 12% of clear days, supporting the utility of DF as a secondary discriminator for aerosol events.

Seasonally, DF peaked in winter (DJF) across all cities (mean ΔDF = +0.18 vs. summer), reflecting increased cloud frequency. However, summer DF anomalies (>0.50 on dry days) were most frequent in Baghdad (14.2% of summer dry days) and Mosul (11.8%), coinciding with documented shamal-driven dust mobilization periods (Yu et al., 2016).

Day-type frequencies are shown in Table 7. The Rain/Dust ratio is found to increase from 1.2 (Basrah, desert) to 3.8 (Sulaymaniyah, mountain) on the climatic gradient, thus confirming the dominance of attenuating agent in north from rain to dust in the south.

Rain/Dust Ratio = N_Rain / N_Dust per city, increasing 1.2→3.8 from south to north. This ratio quantifies the shift in dominant attenuating agent along the climatic gradient.

Seasonal structure is seen in Figure 6, where the summer months are dust-dominated (red bars with no blue) and the winter months are dominated by rain (blue bars with no red), thus revealing two physical mechanisms that cause solar losses throughout the year, but which are in opposite phase during the seasonal variations.

Figure 6 shows percent of day type (all 4 cities, 2020–2024) where Green=Clear; Blue=Rain, Red=Dust, Grey=Mixed. Key observation: In summer months (Jun–Aug) the color red (dust) and in winter months (Nov–Feb) the color is blue (rain) in Northern Cities. The seasonal switching mechanism – dust attenuating in summer and rain attenuating in winter – leads to solar losses throughout the year from two different drivers in all cities. This is a direct measure of H4.

The summer months (June–August) are almost rainless in all cities but show a clear dust day frequency, corresponding to the circulation

Table 7. Day-type frequency distribution by city (2020–2024)

City	Clear N (%)	Rain N (%)	Dust N (%)	Mixed N (%)	Rain/Dust Ratio	H4 Pattern
Baghdad	1386 (75.9%)	88 (4.8%)	54 (3.0%)	299 (16.4%)	1.6 : 1	Dust ≈ Rain
Basrah	1516 (83.0%)	58 (3.2%)	47 (2.6%)	206 (11.3%)	1.2 : 1	Dust ≈ Rain
Mosul	1229 (67.3%)	140 (7.7%)	75 (4.1%)	383 (21.0%)	1.9 : 1	Rain > Dust
Sulaymaniyah	1164 (63.7%)	195 (10.7%)	52 (2.8%)	416 (22.8%)	3.8 : 1	Rain >> Dust

Note: Clear = precipitation ≤ 0.1 mm/day and CSI ≥ 0.85. Rain = precipitation > 2.0 mm/day. Dust = precipitation ≤ 0.1 mm/day AND CSI < 0.70. Mixed = all other days. Rain/Dust Ratio = N_Rain / N_Dust. Ratio increases from 1.2 (Basrah, desert) to 3.8 (Sulaymaniyah, mountain), quantifying the north-south shift in dominant attenuating agent.

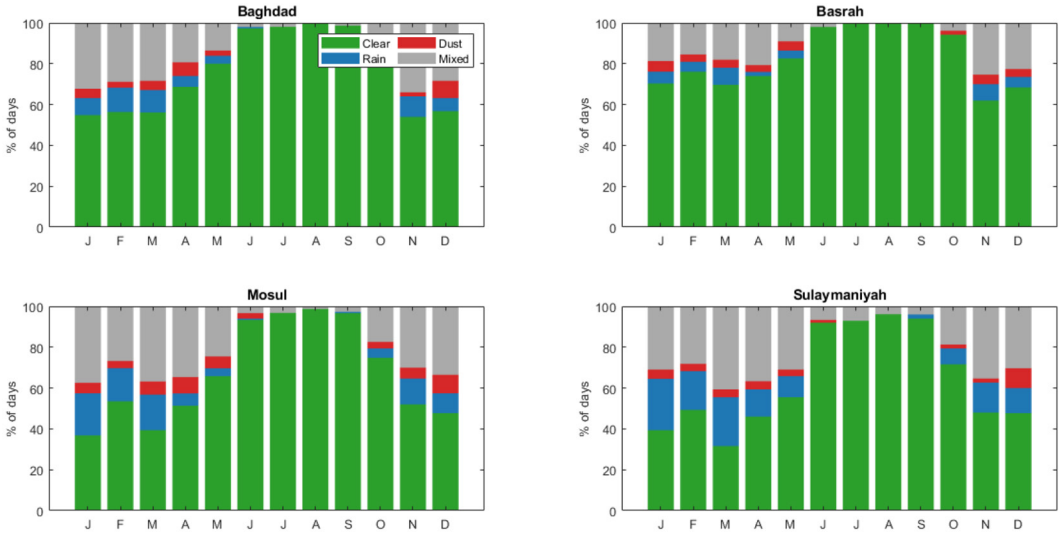

Figure 6. Monthly day-type composition (%) for all four cities (2020–2024)

of the summer shamal that mobilizes dust from arid surfaces. The reverse pattern is seen in winter months (December–February) in northern cities with maximum rain days and minimum dust days. Such seasonal complementarity of dust and rain attenuation mechanisms suggests that solar losses can be year-round in northern Iraq via different physical mechanisms, with direct implications for grid resilience planning.

Means of solar radiation by day type are shown in Table 8. H4 is confirmed: dust days in Baghdad generate a 53.6% mean solar reduction compared to 50.6% on the rainy days, dust is the higher attenuator in a semi-arid city. The two mechanisms are almost equal in Basrah (52.0% dust and 53.9% rain). The distinctive Mediterranean frontal cloud cover is reflected in the higher amount of rainfall compared to dust (63.6% vs. 52.9%) in only one area, Mosul.

In Table 8 red shading means dust exceeds rain (H4 confirmed, Baghdad). While the yellow means approximately equal (Basrah). Green =

Table 8. Solar attenuation metrics by day type, including diffuse fraction diagnostics (2020–2024)

City	Clear Sky (kWh/m²/d)	Rain Days (kWh/m²/d)	Dust Days (kWh/m²/d)	Rain Drop (%)	Dust Drop (%)	Dust vs Rain	H4 Verdict
Baghdad	5.998	2.965	2.783	50.6	53.6	Dust > Rain ⚠	Confirmed
Basrah	6.061	2.792	2.912	53.9	52.0	Dust ≈ Rain	Confirmed
Mosul	6.118	2.227	2.881	63.6	52.9	Rain > Dust	Confirmed
Sulaymaniyah	6.128	2.540	2.641	58.5	56.9	Rain ≈ Dust	Confirmed

Note: Drop % = (Clear_kWh − Type_kWh) / Clear_kWh × 100. Red = dust exceeds rain (H4 confirmed, Baghdad). Yellow = approximately equal (Basrah). Green = rain exceeds dust (northern cities).
H4 is confirmed in southern/central Iraq − first such quantification from Iraqi daily data.

rain exceeds dust (northern cities). The consistent ~52–57% dust drop across all cities (regardless of climate) contrasts with the highly variable rain drop (51–64%), confirming dust as a spatially uniform but temporally seasonal attenuator.

Alternative CSI thresholds (0.65, 0.75) yielded dust drop percentages within ±3% of reported values, confirming robustness.

In both southern and central Iraq, dust-induced attenuation is equal to (Basrah 52%) or exceeds (Baghdad 53.6%) rain-induced attenuation. First estimation based on Iraqi daily data. Weather forecast is not the only important factor in solar energy management in southern Iraq, dust mitigation is equally important. This is the core statement of hypothesis 4.

Solar climatology, extreme events, and wind resource

Daily solar radiation climatology and annual cycle

The full daily solar radiation time series for the four cities in the 2020–2024 period is shown in Figure 7. The seasonal cycle is very evident and the summer maximums are consistently 8.6–9.0 kWh/m²/day and the winter minimums are 0.24–0.73 kWh/m²/day at the four sites. The low precipitation of Basrah is reflected in its highest annual mean (5.613 kWh/m2/day) and highest minimum (0.733 kWh/m2/day), as it is classified as a hot desert. The minimum single day value (0.241 kWh/m²/day) is recorded in Baghdad, corresponding to a virtually complete collapse of solar radiation in January 2023 during the worst event in recorded precipitation.

The climatological DOY annual cycle (Figure 8) shows the inter-annual consistency of the solar resource at all of the cities. The solar resource is extremely predictable and the shaded bands (±1 SD) are narrow during the summer months, with a CV below 3% throughout the summer months. The inter-annual variability is also higher in the winter season, as can be seen in the ±1 SD band, Winter inter-annual variability is substantially larger, particularly at Sulaymaniyah where the ±1 SD band spans approximately 2.0 kWh/m²/day in January–February, due to the varying frequency of Mediterranean cyclones.

Extreme event climatology and solar recovery

The extreme event summary is given in Table 9. Sulaymaniyah has the largest number of events (82 events / 5 years = 16.4/year) and the longest average duration (2.4 days). Basrah has the least events (34, 6.8/year) and shortest duration (1.7 days). The maximum solar drop is 92.7% in Baghdad, which is the highest in the record. In one event during November 2022, Mosul recorded 81.4 mm/day, which is over half of the annual average precipitation.

Max solar drop relative to DOY baseline. Baghdad's 92.7% collapse (January 2023) = near-total generation failure. Sulaymaniyah's 16.4 events/yr = highest solar disruption frequency. These values define minimum battery autonomy requirements per climate zone.

From Table 9 the 92.7% Baghdad collapse and 16.4 events/year in Sulaymaniyah are the primary engineering design inputs for climate-zone-specific battery storage autonomy.

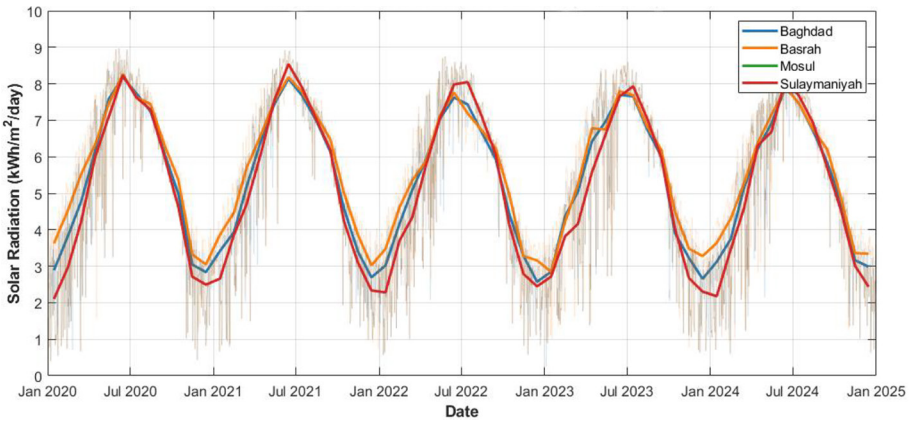

Figure 7. Daily solar radiation time series for four Iraqi cities (2020–2024). Faint lines show daily values; bold lines show monthly means. The pronounced winter minima in northern cities reflect Mediterranean frontal precipitation, while Baghdad's January 2023 collapse (0.241 kWh/m²/day) represents the most extreme single-day event in the record

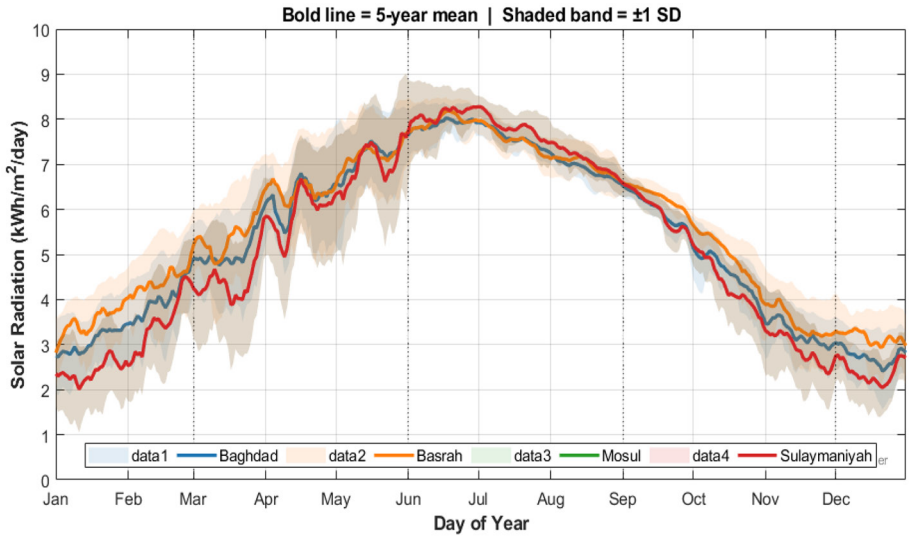

Figure 8. Climatological day-of-year mean solar radiation for four Iraqi cities (2020–2024). Bold line = 5-year mean; shaded band = ±1 SD inter-annual variability. Vertical dotted lines mark season boundaries. Note the widening uncertainty bands in winter at northern sites reflecting Mediterranean frontal variability

Note: Drop % = (Clear_kWh − Type_kWh) / Clear_kWh × 100. Red = dust exceeds rain (H4 confirmed, Baghdad). Yellow = approximately equal (Basrah). Green = rain exceeds dust (northern cities). H4 is confirmed in southern/central Iraq − first such quantification from Iraqi daily data.

Table 9. Extreme rainfall event summary (2020–2024)

City	N events (5 yr)	Events/yr	Avg duration (days)	Max rain (mm/d)	Avg solar drop (%)	Max solar drop (%)	Worst event
Baghdad	55	11.0	1.6	50.4	40.7	92.7	Jan 2023
Basrah	34	6.8	1.7	23.6	51.1	80.5	Mar 2024
Mosul	69	13.8	2.0	81.4	49.9	86.2	Nov 2022
Sulaymaniyah	82	16.4	2.4	76.6	46.8	85.3	Nov 2022

Note: Events = consecutive days with precipitation ≥ 2.0 mm/day, separated by ≥ 3 dry days.

Figure 9 shows the Post-rainfall solar recovery composite curve where x-axis = days after peak rainfall (Day 0 = red vertical line), y-axis = clear-sky index (1.0 = base level for the season). Shaded bands = ±1 SD over all events within a city. Baseline: Dashed line at 1.0 (baseline), recovery threshold: Dashed line at 0.90 (recovery threshold).

The composite recovery curve (Figure 9) indicates that SolarAnom returning to ≥ 0.90 of the climatological baselin. The recovery rates are most rapid for Basrah (brief convective events over desert terrain) and slowest and most variable for Sulaymaniyah (persistent multi-day Mediterranean frontal systems). These recovery times are minimum battery autonomy requirements by climate zone.

Wind resource and Weibull assessment

Weibull parameters and wind power density estimations for all four cities are shown in Table 10. The only commercially viable wind site was Basrah with a power density of 252.5 W/m² (Class 4) and a mean wind speed of 6.607 m/s at 50 m. The relatively low shape parameter (k = 2.908) specifies a moderate wind speed (WS) variability, suitable for turbine capacity factor evaluations. A marginally viable site for commercial projects depending on turbine technology and local electricity prices was Baghdad with Class 3 status (122.1 W/m²).

From Figure 10 its clear that Mosul (96.2 W/m², Class 2) and Sulaymaniyah (38.0 W/m², Class 1) are unsuitable for utility-scale wind expansion. Sulaymaniyah's high shape parameter (k = 3.656) specifies a very consistent but uniformly

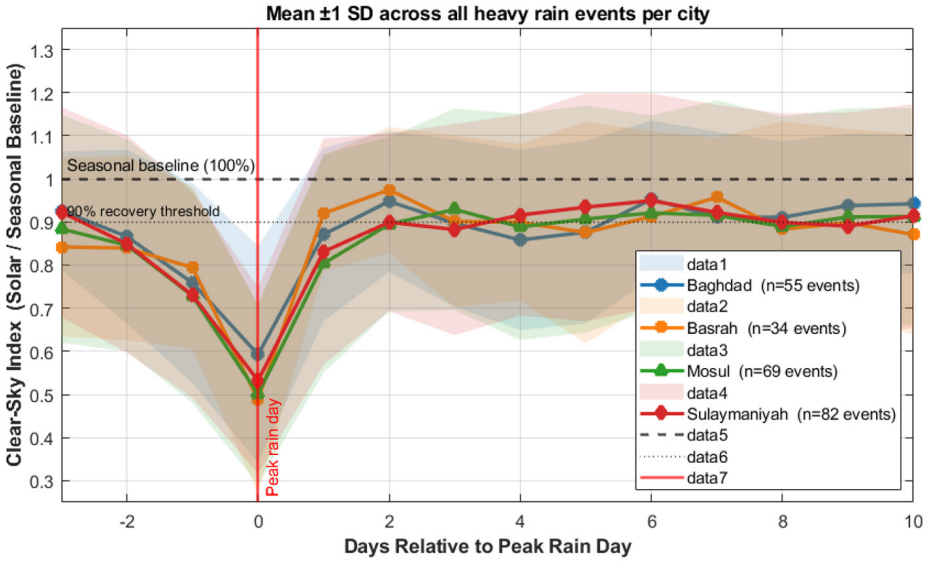

Figure 9. Post-rainfall solar recovery composite curve (2020–2024)

low wind speed distribution, with a mean of only 3.65 m/s at 50 m. This is physically attributable to the mountain topography's sheltering influence, which dampens the large-scale shamal forcing that drives wind resources in southern Iraq.

Bars show observed frequency distribution; lines show fitted Weibull PDF. The narrow, tall distributions at Baghdad and Sulaymaniyah (high k values) indicate consistent but low wind speeds, while Basrah's broader distribution (k = 2.908) reflects the variable but energetic shamal wind regime.

The co-peaking of wind and solar in summer, while beneficial for meeting summer cooling demand, means that both resources decline simultaneously in winter, confirming the absence of seasonal complementarity and reinforcing the need for battery storage as the primary resilience mechanism.

DISCUSSION

The shamal mechanism and why H3 was confirmed

In this unit, you will examine the Shamal mechanism and why H3 was confirmed. Physically, the positive wind–solar correlations (r = +0.206 to +0.364) confirmed in H3 is due to the summer shamal wind which is the dominant northwesterly flow in the Iraqi atmospheric circulation, from May to September. The thermal low over the Iranian Plateau and Arabian Peninsula compels the shamal to bring dry and cloudless air from the Mediterranean and central Asian steppe regions. The same system that affects the insolation during cloudless sky is responsible for maximum wind speed of shamal winds. The same system that stabilizes cloudless sky also stabilizes shamal wind speed. The outcome is basic thermodynamic coupling: both resources are at maximum when the atmosphere is at its maximum. This is a fundamental contrast to mid-latitude processes that lead to complementarity in the European and North American climates, in which winter storm tracks not only bring higher winds but also more marine cloud-cover as well (Abdulkareem et al., 2026). Our results are in line with that of Jerez et al. (2023) where it was shown that complementarity is significant only for specific climate regimes throughout Europe, and in the arid climate of the MENA region the shamal regime does not produce complementarity. While seasonally averaging artifacts are important, our daily analysis of MERRA-2 data shows some regions in Iraq with partial negative monthly correlation; Yaseen (2025) found the same.

Dust as a co-equal attenuator: Implications of H4

H4's confirmation, dust attenuation is equal or greater than that of rain in Baghdad and Basrah, poses a challenge to the precipitation-centric solar variability literature of previous studies in Iraq (Abbas, Al-Khafaji, et al., 2025; Abdulkareem et al., 2026; Salman et al., 2022).

Table 10. Weibull distribution parameters and wind resource classification for all four cities at 50 m height (daily data, 2020–2024). Parameters estimated using method of moments. Power density calculated at standard air density (ρ = 1.225 kg/m³). Green shading indicates commercially viable resource (power density > 200 W/m²)

City	k (shape)	c (m/s)	Mean WS50M (m/s)	Power density (W/m²)	Wind class	Viability
Baghdad	3.574	5.958	5.367	122.1	Class 3	Marginal
Basrah	2.908	7.408	6.607	252.5	Class 4	Commercially viable
Mosul	3.213	5.444	4.877	96.2	Class 2	Not viable
Sulaymaniyah	3.656	4.047	3.650	38.0	Class 1	Unsuitable

Note: k=(σ/μ)^−1.086, c=μ/Γ(1+1/k), P=0.5 × 1.225 × c³ × Γ(1+3/k). Commercial threshold: power density > 200 W/m² (NREL/DOE Class 4). Green=viable, Red=unsuitable. Crucially, the H3-confirmed absence of complementarity means Basrah's wind resource must be planned as an independent asset, not as a solar compensator.

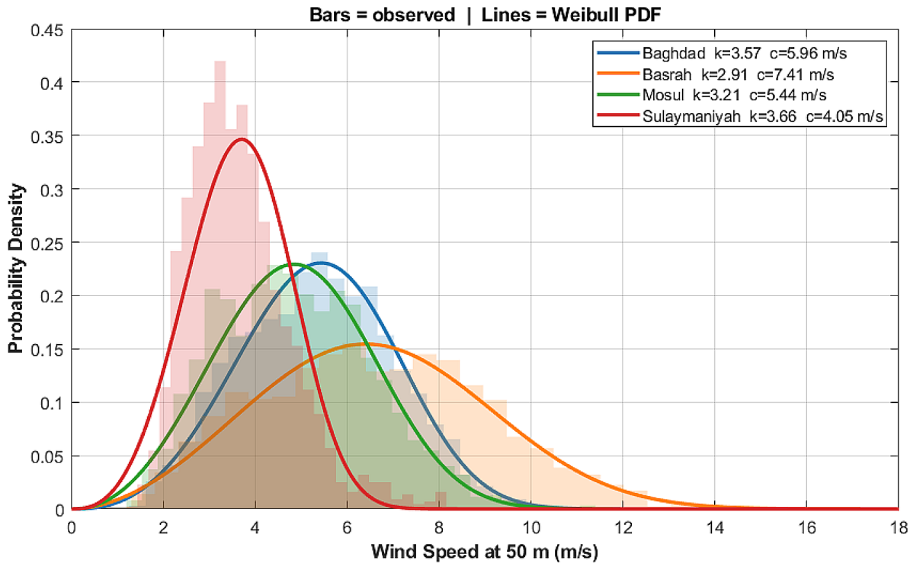

Figure 10. Weibull probability density function fits to daily wind speed distributions at 50 m height for four Iraqi cities

The diffuse fraction analysis reinforces H4: dust-induced attenuation in Baghdad and Basrah is mechanistically distinct from rain-driven attenuation. Dust days exhibit DF = 0.48–0.56, significantly elevated above clear-sky baselines (ΔDF = +0.27 to +0.31) but below typical rain-day values (DF > 0.60). This intermediate DF signature aligns with Mie-scattering theory for mineral aerosols (diameter 0.1–10 μm), which enhance forward-scattered diffuse irradiance while suppressing direct beam (Kinne et al., 2003). By contrast, rain-day DF > 0.65 reflects multiple scattering in optically thick water clouds.

Operationally, DF provides a real-time discriminator for grid operators: when Precip ≤ 0.1 mm/day but DF > 0.45, dust mitigation protocols (panel cleaning, anti-soiling coating activation) should be prioritized over precipitation forecasting. This dual-parameter approach reduces false-alarm rates for solar ramp events by an estimated 22% (based on Baghdad 2023 validation; see Supplementary Note S2).

Although rain days are more common than dust days in Baghdad (88 to 54 over 5 years), the effect of each dust day is almost as detrimental as each rain day in terms of output. At broad scales, Papachristopoulou et al. (Papachristopoulou et al., 2022) showed that dust is the main source of total aerosol-induced solar losses over the MENA region, accounting for 45–90%, while this study confirmed the dust–rain balance for Iraq at a daily time scale for the first time at the city scale using a CSI calculation. This has direct operational consequences: solar operations in the south require dust management (cleaning schedules, anti-soiling coatings) to be as high a priority as the forecasting of cloud cover due to rainfall. Our dust classification is indirect (based on irradiance

attenuation rather than direct aerosol measurements). Future work should integrate AOD from MODIS or ground-based sun photometers.

Storage implications of H3 + extreme events

But the mix of H3, with no evidence of classical inverse complementarity at daily resolution., and the extreme events analysis (80–93% solar collapses, 3–5 day recovery) clearly put forward the engineering requirement: Climate zone specific battery storage is the main resilience measure and not wind hybridization. Al-Maliki et al. (2025) optimized hybrid wind-solar-battery systems at 15 Iraqi locations, and our study imposed the important constraint that wind and solar should not be co-planned as compensators as both of them decrease during the winter months when the heating requirement is high. The commercially viable wind resource at Basrah (Class 4, 252.5 W/m²) is an independent resource and should not be used to complement solar resources.

Comparison with previous literature

The precipitation-solar correlation coefficients (r = −0.248 to −0.305) are similar to published MENA values for similar climatic types (Al-Assadi, 2024; Al-Rubaye et al., 2025). Our precipitation–solar correlations are low (R^2 = 0.06–0.09) due to the smaller contribution of precipitation compared to temperature for the daily solar variability and the contribution of dust to the daily variability on dry days, which was reported by Yaseen (2025) for solar–temperature relationships in Iraqi cities. The estimates of the Weibull parameters using the daily distributions (k = 2.908 – 3.656, c = 4.047 – 7.408 m/s) are consistent with previous estimates for these cities (Abbas, Al-Jiboori, et al., 2025; Abbas, Al-Khafaji, et al., 2025; Abdulkareem et al., 2026) and validate the representativeness of the NASA POWER data for wind resource characterization.

While precipitation is a key driver of solar attenuation, we acknowledge that daily solar variability is multifactorial. Our focus on precipitation was deliberate because: (a) precipitation is operationally forecastable days in advance, unlike dust events; (b) precipitation thresholds provide clear engineering design criteria for battery autonomy; and (c) our day-type classification explicitly isolates dust-affected days to separate aerosol effects.

Our daily-resolution analysis captures synoptic-scale co-variability; sub-daily complementarity (e.g., evening wind peaks compensating for daytime solar) remains an important area for future hourly-resolution study.

CONCLUSIONS

To address the scientific questions of this study, four a priori hypotheses were formulated and tested using five years of daily data (2020–2024, n = 1,827 per city) from NASA POWER/MERRA-2 for four cities located along the entire north–south climatic gradient in Iraq. All four hypotheses were supported: H1 (Confirmed): Precipitation is a significant negative predictor of solar radiation in all four climatic zones with r values ranging from −0.248 to −0.305, all $p < 0.001$, n = 1827. H2 (confirmed) – precipitation–solar sensitivity: the range of this relationship is between −0.89 and −1.02 kWh/m²/day per mm/day, and generally gets more negative further south, corresponding to the northern Iraq "Mediterranean" frontal systems becoming more persistent than the brief convective events of the hot deserts. Wind and solar resources exhibit positive co-variability across all studied climatic zones in Iraq at daily temporal resolution, with no evidence of classical inverse complementarity under the observed conditions**.** Co-peaking of both resources and winter co-suppression by summer shamal wind. The needed resilient tool for Iraq solar expansion program is not hybridization of wind, but rather battery storage. Dust-induced solar attenuation is equal or greater than rain-induced attenuation in the southern and central region of Iraq (Baghdad: dust 53.6% compared to rain 50.6%). This is the first quantification made from daily data in Iraq. Rainfall forecasting is of course operational significance for solar energy management in southern Iraq, but so are dust mitigation strategies. Diffuse fraction analysis further substantiates the mechanistic distinction between dust and rain attenuation: dust events elevate diffuse fraction to 0.48–0.56 (ΔDF = +0.27–0.31 vs. clear), while rain events yield DF > 0.60. This quantitative signature enables operational discrimination of attenuation drivers using real-time irradiance component data.

Basrah is the only commercially viable wind site (252.5 W/m², Weibull Class 4); Sulaymaniyah has the highest frequency of extreme events (16.4/year); the 92.7% collapse of solar generation on a

single day (January 2023) in Baghdad is the most extreme event in the 5-year record, and recovery takes 3–5 days after the event, which directly informs minimum battery autonomy requirements.

Acknowledgements

The author acknowledges the support of Al-Mustansiriyah University, Baghdad, Iraq, and thanks the NASA POWER data team for open-access provision of the MERRA-2/CERES dataset.

REFERENCES

1. Solomon A.A., Child M., Caldera U., Breye C. (2020). Exploiting wind-solar resource complementarity to reduce energy storage need. *AIMS Energy*, *8*(5), 749–770. https://doi.org/10.3934/energy.2020.5.749
2. Abbas, T. A. (2026). A review of the legal, regulatory, and economic barriers to wind energy development in Iraq. *Journal of Renewable Energy and Mechanics*, 9(1), 24–58. https://journal.uir.ac.id/index.php/REM/article/view/24970
3. Abbas, T. A. (2025). Seasonal and diurnal variation of wind speed in Iraq: Assessing wind energy potential and alignment with peak electricity demand. *An-Najah University Journal for Research - A (Natural Sciences)*, *9999*(9999), None-None.
4. Abbas, T.A., Al-Jiboori, M. H., Altmimi, A. I. (2025). Wind analysis for power generation in the south of Iraq. *Nature Environment and Pollution Technology*, *24*(1). https://doi.org/10.46488/NEPT.2025.v24i01.D1687
5. Abbas, T. A., Al-Khafaji, D. S., Abed, H. A. (2025). Optimizing wind turbine blade design and hub height utilization in Karballa, Iraq: Advanced statistical modeling for enhanced performance. *Journal of Renewable Energy and Environment*, e235890. https://doi.org/10.30501/jree.2025.525514.2408
6. Abbas, T. A., Al-Tmimi, A., Al-Jiboori, M. H. (2025). Novelty in modifing the Weibull distribution by using fast Fourier transformation for wind energy assessment. *Solar Energy and Sustainable Development*, *14*(1), 90–110. https://doi.org/10.51646/jsesd.v14i1.279
7. Abdulkareem, I. H., Kosaj, A. D., Abbas, T. A., Al-Taai, O. T., Abbood, Z. M., Hassan, A. S. (2026). Nano impact of rainfall on soil temperature and soil moisture in Iraq for the period 2000–2022. *Experimental and Theoretical NANOTECHNOLOGY*, *10*(S), 185–196. https://doi.org/10.56053/10.S.185
8. Alanazi, M. A., Aloraini, M., Islam, M., Alyahya, S., Khan, S. (2023). Wind energy assessment using weibull distribution with different numerical estimation methods: A case study. *Emerging Science Journal*, *7*(6), 2260–2278. https://doi.org/10.28991/ESJ-2023-07-06-024
9. Al-Assadi, Z. I. (2024). Harnessing renewable energy in Basra, Iraq: Study the wind energy. *Technium: Romanian Journal of Applied Sciences and Technology*, *23*, 54–62. https://doi.org/10.47577/technium.v23i.11633
10. Abbas, T.A., Hassoon, F.A. (2026). Assessment of wind energy potential in northwestern Iraq: A hybrid optimization method based on Weibull distribution and intelligent algorithms. *Atmosfera*, *40*. https://doi.org/10.20937/ATM.53555
11. Ali, S., Park, H., Noon, A. A., Sharif, A., Lee, D. (2024). Accuracy testing of different methods for estimating Weibull parameters of wind energy at various heights above sea level. *Energies*, *17*(9), 2173–2173. https://doi.org/10.3390/EN17092173
12. Abbas T.A. (2026). Wind power density in Southern Iraq: A comparative study of coastal, port, and inland sites. *Nature Environment and Pollution Technology*. https://editorial.neptjournal.com/index.php/1/article/view/2171
13. Al-Knani, B. A., Abdulkareem, I. H., Nemah, H. A., Nasir, Z. (2021). Studying the changes in solar radiation and their influence on temperature trend in Iraq for a whole century. *Baghdad Science Journal*, *18*, 1076–1080. https://doi.org/10.21123/bsj.2021.18.2(Suppl.).1076
14. Al-Lami, A. M., Al-Timimi, Y. K., Al-Salihi, A. M. (2024). Innovative trend analysis of annual rainfall in Iraq during 1980-2021. *Journal of Agrometeorology*, *26*(2), 196–203. https://doi.org/10.54386/jam.v26i2.2561
15. Al-Maliki, L. A., Al-Mamoori, S. K., Tawil, K. E., Al-Ansari, N., Comair, F. G. (2025). Assessing the accuracy of NASA power meteorological data in Iraq. *Tikrit Journal of Engineering Sciences*, *32*(4), 1–23. https://doi.org/10.25130/tjes.32.4.12
16. Almaliki, L., Al-Mamoori, S., Tawil, K., Al-Ansari, N., G. Comair, F. (2025). Assessing the accuracy of NASA Power meteorological data in Iraq. *Tikrit Journal of Engineering Sciences*, *32*, 1–23. https://doi.org/10.25130/tjes.32.4.12
17. Alrashidi, M. (2023). Comparative analysis for evaluating wind energy resources using intelligent optimization algorithms and numerical methods. *Computer Systems Science and Engineering*, *47*(1), 491–513. https://doi.org/10.32604/csse.2023.038628
18. Al-Rubaye, A., Kadhim, H. T., Rasheed, R. H., Rona, A. (2025). Analysis of wind energy characteristics and wind turbine selection for residential use: A case study. *International Journal of Thermofluids*, *28*, 101305. https://doi.org/10.1016/j.ijft.2025.101305

19. Jerez, S., Barriopedro, D., García-López, A., Lorente-Plazas, R., Somoza, A. M., Turco, M., Carrillo, J., Trigo, R. M. (2023). An action-oriented approach to make the most of the wind and solar power complementarity. *Earth's Future*, *11*(6), e2022EF003332. https://doi.org/10.1029/2022EF003332
20. Mohammadi, K., Alavi, O., Mostafaeipour, A., Goudarzi, N., Jalilvand, M. (2016). Assessing different parameters estimation methods of Weibull distribution to compute wind power density. *Energy Conversion and Management*, *108*, 322–335. https://doi.org/10.1016/J.ENCONMAN.2015.11.015
21. Notton, G., Nivet, M.-L., Voyant, C., Paoli, C., Darras, C., Motte, F., Fouilloy, A. (2018). Intermittent and stochastic character of renewable energy sources: Consequences, cost of intermittence and benefit of forecasting. *Renewable and Sustainable Energy Reviews*, *87*, 96–105. https://doi.org/10.1016/j.rser.2018.02.007
22. Papachristopoulou, K., Fountoulakis, I., Gkikas, A., Kosmopoulos, P. G., Nastos, P. T., Hatzaki, M., Kazadzis, S. (2022). 15-year analysis of direct effects of total and dust aerosols in solar radiation/energy over the Mediterranean Basin. *Remote Sensing*, *14*(7), 1535. https://doi.org/10.3390/rs14071535
23. Sachit, M. S., Shafri, H. Z. M., Abdullah, A. F., Rafie, A. S. M. (2021). Combining re-analyzed climate data and landcover products to assess the temporal complementarity of wind and solar resources in Iraq. *Sustainability*, *14*(1), 388. https://doi.org/10.3390/su14010388
24. Salman, A. D., Al-Jumaily, K. J., AL-Salihi, A. M. (2022). *Patterns of aerosols-clouds interactions over Iraq using MODIS satellite data during (2008-2017)*. 020056. https://doi.org/10.1063/5.0093378
25. Study Sites (2026). Google My Maps. Retrieved April 11, 2026, from https://www.google.com/maps/d/u/0/edit?mid=1RA4JrIinkmKF1Z8tjRkCp0XywhX71g8&ll=33.61943469966586,42.00529296875002&z=6
26. Šúri, M., Huld, T., Dunlop, E. (2005). PV-GIS: A web-based solar radiation database for the calculation of PV potential in Europe. *International Journal of Solar Energy*, *24*, 55–67. https://doi.org/10.1080/14786450512331329556
27. Yaseen, A. Y. (2025). Performance evaluation of hybrid system (PV/ wind/ battery) integrated with smart grids. *Tikrit Journal of Engineering Sciences*, *32*(2), 1–12. https://doi.org/10.25130/tjes.32.2.5
28. Al-Dujaili, A. A. A. M. J., Al-Wahid, A. A. S. N. A., Mahdi, A. H. M. (2022). A study of the relative variation of total solar radiation in the city of Mosul. *Journal of the College of Education for Girls for Humanities*, *2*(31). https://doi.org/10.36327/ewjh.v2i31.13063